Intramolecular Dynamics of Tetranuclear Iridium Carbonyl Cluster Compounds

Part VI[1])

Derivatives with Bidentate Ligands. Crystal Structures of *tetrahedro*-Decacarbonyl{μ-[1,1-bis(methylthio-$\varkappa S$)ethane]}tetrairidium ([$Ir_4(CO)_{10}$-(μ_2-$(MeS)_2$)CHMe)]), *tetrahedro*-Tri-μ-carbonylheptacarbonyl{μ-{ethylidenebis[diphenylphosphine]-$\varkappa P$: $\varkappa P'$}}tetrairidium ([$Ir_4(CO)_{10}$(μ_2-$(Ph_2P)_2$CHMe)]), and *tetrahedro*-Tri-μ-carbonylheptacarbonyl{μ-{propane-1,3-diylbis[diphenylphosphine]-$\varkappa P$: $\varkappa P'$}}tetrairidium ([$Ir_4(CO)_{10}$(μ_2-$Ph_2P(CH_2)_3PPh_2$)])

by **Tito Lumini**, **Gábor Laurenczy**, and **Raymond Roulet***

Institut de Chimie minérale et analytique de l'Université, BCH, CH-1015 Lausanne

and **Augusto Tassan** and **Renzo Ros**

Dipartimento di Processi Chimici dell'Ingegneria e Centro di Chimica Metallorganica del CNR, Via Marzolo 9, I-35131 Padua

and **Kurt Schenk**

Institut de cristallographie de l'Université, BSP, CH-1015 Lausanne

and **Giuliana Gervasio***

Dipartimento di Chimica I.F.M., Via Giuria 7, I-10125 Torino

The disubstituted clusters [$Ir_4(CO)_{10}(\mu_2$-L–L)] with one edge-bridging ligand have a ground-state geometry with all COs terminal (L–L = $(MeS)_2$CHMe, cluster **1**) or with three edge-bridging COs (L–L = $(Ph_2P)_2$CHMe, cluster **2**; L–L = $Ph_2P(CH_2)_3PPh_2$, cluster **3**) in the solid state and in solution. A comparative ^{13}C-NMR study of **1**–**3** shows that their respective ground-state geometries are merely relative minima of energy in the same kinetic profile of successive fluxional processes consisting of a merry-go-round of six COs about a unique triangular face and the rotation of terminal COs about one Ir-atom. The factors affecting the activation energy of the merry-go-round result from the relative bites of the bidentate ligands in the ground-state geometry, as shown by a comparison of the molecular structures of **2** and **3**.

Introduction. – In a preceding article of this series [2], we proposed that the fluxional processes taking place in the disubstituted clusters [$Ir_4(CO)_{10}(\mu_2$-L–L)] with one edge-bridging ligand and with a ground-state geometry with three edge-bridging COs were a merry-go-round of six COs about a unique triangular face followed by the rotation of terminal COs bonded to two Ir-atoms residing on the mirror plane of a postulated unbridged intermediate. For P and As bidentate donor ligands (L–L = bis(diphenylphosphino)methane (= methylenebis[diphenylphosphine]), bis(diphenylarsino)methane

[1]) Part V: [1]

(= methylenebis[diphenylarsine]), and bis(diphenylphosphino)propane (= propane-1,3-diylbis[diphenylphosphine])), these intermediates were not observed. The aim of the present study was to find a system where the unbridged geometry is that observed for the ground state, and which would display the same kinetic profile as the one proposed for the clusters with P and As donor ligands. The cluster $[Ir_4(CO)_{10}(\mu_2\text{-}(MeS)_2CHMe)]$ was found to have the desired geometry both in the solid state and in solution. A comparative ^{13}C-NMR study of this cluster and of $[Ir_4(CO)_{10}(\mu_2\text{-}(Ph_2P)_2CHMe)]$ was therefore undertaken. The crystal structures of these two clusters and of $[Ir_4(CO)_{10}(\mu_2\text{-}Ph_2P(CH_2)_3PPh_2)]$ are also reported, as well as a proposed correlation between a structural factor of the ground states and the relative activation energies of the merry-go-round proces.

Crystal Structures of $[Ir_4(CO)_{10}(\mu_2\text{-}(MeS)_2CHMe)]$ (1), $[Ir_4(CO)_{10}(\mu_2\text{-}(Ph_2P)_2CHMe)]$ (2), and $[Ir_4(CO)_{10}(\mu_2\text{-}Ph_2P(CH_2)_3PPh_2)] \cdot {}^1/_2C_6H_6$ (3). – The preparation of **3** had already been reported [2]. Single crystals were obtained by diffusion of a layer of hexane in CH_2Cl_2 at $-25°$ for **1** and **2**, and by slow evaporation at room temperature of a solution in benzene/heptane 1:5 for **3**.

The crystals consist of discrete molecules, without abnormally close intermolecular contacts, except for **2**. The overall structures of **1**–**3** and the labelling schemes are shown in *Figs. 1–3*. Some relevant interatomic distances and angles are reported in the *Exper. Part*. Lists of atomic fractional coordinates and other crystallographic data are available as supplementary material.

The molecule of **1** has practically C_s symmetry and contains a nearly tetrahedral metal core with terminal CO ligands only. It is one of the few examples [3] of substituted Ir_4

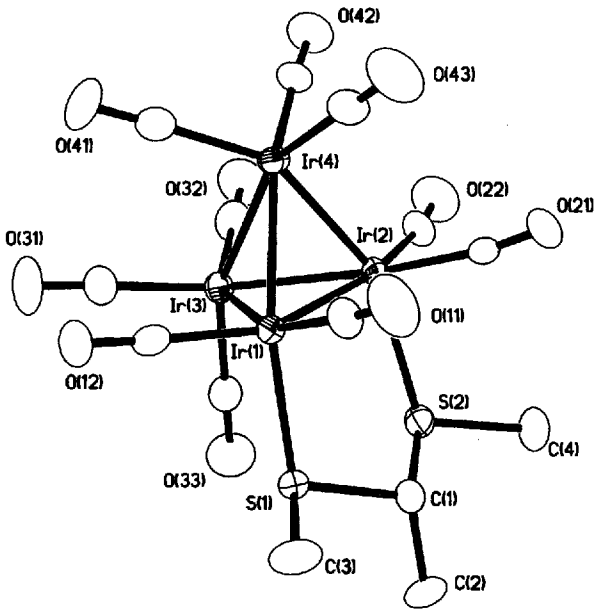

Fig. 1. *ORTEP View of the molecular structure of* **1**. Thermal ellipsoids at 30% probability.

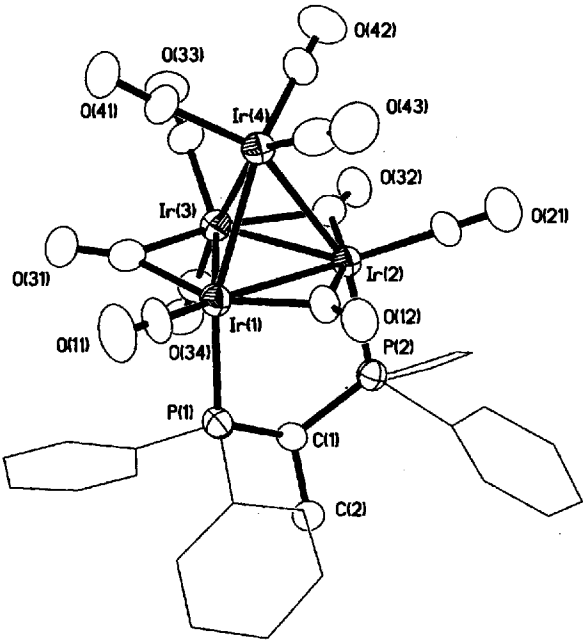

Fig. 2. *ORTEP View of the molecular structure of* **2**. Thermal ellipsoids at 30% probability.

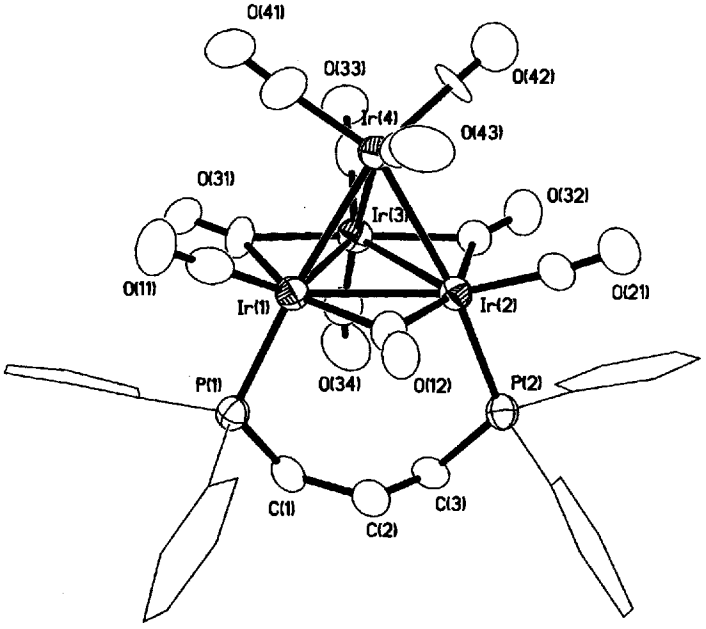

Fig. 3. *ORTEP View of the molecular structure of* **3**. Thermal ellipsoids at 30% probability.

clusters devoid of bridging COs. The shortest Ir–Ir bond distance (2.6515(6) Å) is that spanned by the bridging ligand with a difference of 50 σ relative to the mean value of the six Ir–Ir distances (2.6796(7) Å). The Ir–S bond distances can only be compared to those found in the CO-unbridged isomer of $[Ir_4(CO)_9(\mu_3\text{-}1,3,5\text{-trithiane})]$ [4] (mean values of 2.381(5) and 2.354(5) Å, resp.). The S-atoms of the bridging ligand are in axial positions with respect to the Ir(1)–Ir(2)–Ir(3) plane with a S(1)···S(2) distance of 2.93 Å, and the Ir–S bonds form an angle of 95° (mean value) with respect to this plane. The axial Ir(3)–C(33) bond forms a corresponding angle of 98°. All Ir–C and C–O bond distances are in the normal range of values found for terminal CO groups; the tilt angles of COs out of the basal plane towards Ir(4) are in the range 12–17°, with the exception of CO(31) (2°). In the five-membered ring formed by the bridging ligand, the out-of-plane C(1) atom can give rise to two conformations: in conformation **A**, this C-atom points towards the outside of the cluster, in conformation **B**, C(1) points towards the axial CO on Ir(3). Each of these arrangements can give rise to two isomers **a** and **b** if the Me group and the H-atom are interchanged (see **A** and **B**, X = S, P).

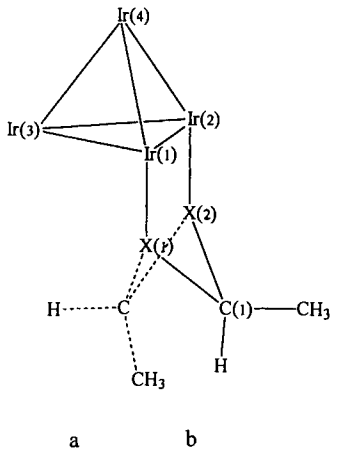

a b

Conformers **A**

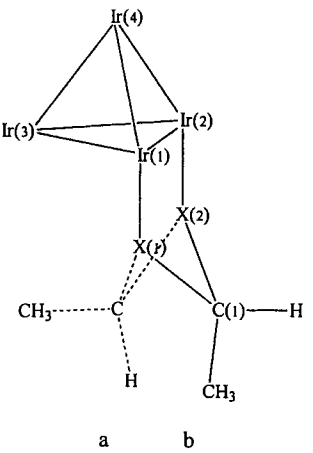

a b

Conformers **B**

The four arrangements **A** and **B** have a mirror plane passing through C(1) and Ir(3) and Ir(4); that adopted by the bridging ligand in complex **1** is such that the C–Me bond is about parallel to the S(1)–Ir(1)–Ir(2)–S(2) plane, C(1) and the H-atom at C(1) point outwards (see **Bb**).

In contrast to **1**, clusters **2** and **3** have three edge-bridging COs defining the basal face (Ir(1)–Ir(2)–Ir(3)); the bidentate ligand is in axial position with respect to that face. Complex **2** corresponds to conformation **Aa**, *i.e.*, the conformation adopted by the bridging ligand in **2** is such that the C–Me bond is about parallel to the Ir(1)–Ir(2)–Ir(4) face (rather than to the basal face). This is not the only conformation observed in solution (see *Exper. Part*).

Complex **3** has C_s symmetry including the Ph moieties, with a mirror plane passing through Ir(3), Ir(4), and the mid-point of the Ir(1)–Ir(2) bond; in complex **2**, the phenyl substituents at P(1) and P(2) are not related by a mirror plane. Why? *Fig. 4* shows

space-filling models of the two molecules **2** and **3** with a view nearly perpendicular of the Ir(1)–Ir(2)–P(1)–P(2) plane. The difference could be due to intramolecular steric hindrance; however, the energy profiles of the scans around the P–C_6H_5 bond of the phenyl group I of complex **2**, calculated with the aid of the simple force field provided by the MOLDRAW program [5], show that both the symmetric and asymmetric forms lie in a energy minimum. A close inspection of the intramolecular interactions in the two complexes shows that O(12) interacts similarly with the H-atoms evidenced in *Fig. 4* (O(12)···H(16) 2.38 Å in **2**; O(12)···H(9) 2.30 Å, O(12)···H(17) 2.50 Å in **3**). The asymmetry of complex **2** must, therefore, be attributed to an intermolecular interaction; in fact, in close interaction O(12)···H(11) (2.43 Å) with a neighbouring molecule may prevent the symmetric arrangement.

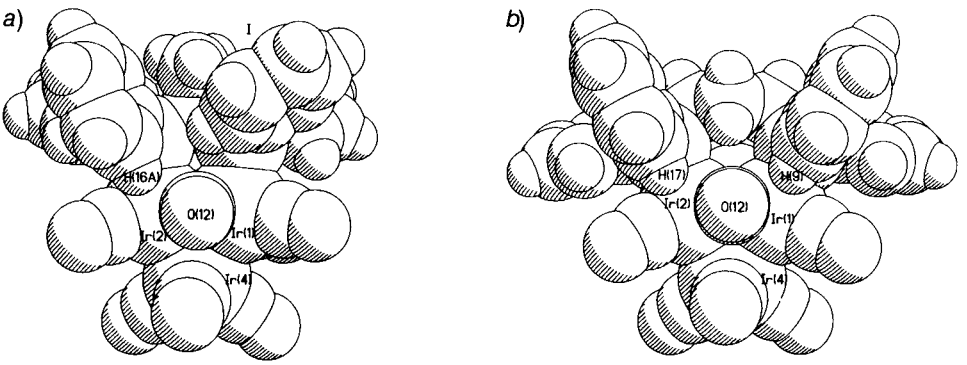

Fig. 4. *Space-filling models of* a) **2** *and* b) **3** *in a view nearly perpendicular to the Ir(1)–Ir(2)–P(1)–P(2) plane*

The two molecules **2** and **3** have symmetrically bridging COs, as the Ir–C distances deviate at most by 5 σ for **2** and 3 σ for **3** from their respective mean values. In **2**, the Ir–Ir bond spanned by the bridging ligand (2.701(1) Å) is the shortest one with a difference of 28 σ relative to the mean value of the six Ir–Ir distances (2.729(1) Å), whereas it is the longest (2.775(2) Å) in **3** with a difference of 16 σ relative to the corresponding mean value (2.738(2) Å). The angles between the Ir–P bonds and the basal plane have values of 101 and 116° in **2** and **3**, respectively. Both differences reflect the significantly smaller bite of the coordinated ligand in **2** (P(1)···P(2) = 3.20 Å) relative to that in **3** (P(1)···P(2) = 4.66 Å) which has a longer C-chain. The different bites of the coordinated ligands have an effect on the tilt angle of the basal carbonyl ligands relative to the basal plane towards the apical Ir-atom.

The averaged tilt angle of Ir(1)–C(11) or Ir(2)–C(21) with respect to the basal plane has values of 18 and 27° in **2** and **3**, respectively (the values of the tilt angle of C(33) should not be compared due to different interactions of the rigid group C(33)–Ir(3)–C(34) with the Ph groups). The opposite trend is observed for the tilt of the Ir(1)–Ir(2)–C(12) plane with respect to the basal plane (12 and 3° for **2** and **3**, resp.). Another consequence of the different bites is that the Ph groups are pushed down further away from the basal plane in **2** compared to **3**, *e.g.* the distances of the center of the benzene ring closest to the COs bearing atoms O(11) and O(31) have values of 5.5 and 4.2 Å in **2**, respectively, and of 4.8 and 3.5 Å in **3**. We believe that these structural factors are related to the energies of the merry-go-round process in **2** and **3** (see below).

Fluxional Behaviour of Clusters 1–3 in Solution. – The reaction of $[Ir_4(CO)_{11}Br]^-$ with 1,1-bis(methylthio)ethane (*ca.* 5 mol-equiv.) in the presence of $AgBF_4$ (*ca.* 1 mol-equiv.) in cold CH_2Cl_2, followed by prep. TLC, gave two fractions consisting of **1** (55%) and $[Ir_4(CO)_{11}(MeS)_2CHMe-\varkappa S)]$ (12%). The latter cluster is unstable in solution at room temperature due to disproportionation into **1** and insoluble $[Ir_4(CO)_{12}]$.

The limiting ^{13}C-NMR spectrum of a sample of **1** enriched in ^{13}CO (*ca.* 25%) in CD_2Cl_2 at 177 K consists of six resonances in the region of terminal COs, at 167.7(*a*), 164.9(*b*), 164.1(*c*), 158.8(*d*), 157.2(*g*), and 154.3(*e*) ppm, with relative intensities 2:2:1:2:2:1 (see below, *Fig. 6,a*). Its ^1H-NMR spectrum shows only 1 *q* and 1 *d* for the H–C–Me group indicating only one conformation of the coordinated bidentate ligand. The presence of 1 *s* for the two MeS groups confirms the mirror symmetry of the molecule. Therefore, the ground-state geometry of **1** in solution is similar to the structure in the solid. The assignment of the CO resonances was based on a 2D-COSY at 178 K in CD_2Cl_2 showing cross-peaks between the resonances at 164.9 and 158.8 ppm, and between the resonances at 164.1 and 154.3 ppm due to pseudo-*trans* couplings and by comparison with the ^{13}C-NMR spectrum of $[Ir_4(CO)_9(\mu_3\text{-}1,3,5\text{-trithiane})]$[4].

A 2D-EXSY spectrum of **1** at 212 K in CD_2Cl_2 shows intense cross-peaks indicating the dynamic connectivities $b \leftrightarrow a \leftrightarrow d$ (see *Fig. 5*). The cross-peak between the resonances at 164.9 and 158.8 ppm is of second-order, excluding a direct exchange $b \leftrightarrow d$. A less intense, first-order cross-peak is also observed between the resonances at 164.1 and 158.8 ppm indicating the exchange $c \leftrightarrow d$. At *ca.* 270 K, a third exchange, $g \leftrightarrow e$, becomes apparent. The unbridged ground state is, therefore, the place of three successive site exchanges. The exchange $b \leftrightarrow a \leftrightarrow d$ is clearly the merry-go-round of six COs about a unique triangular face (the face Ir(1)–Ir(2)–Ir(3) in *Fig. 1*). Both, the second and third exchanges involve only two sites and must correspond to the rotation of three COs about a local C_3 axis passing through each of the two Ir-atoms residing on the mirror plane of the molecule (Ir(3) and Ir(4) in *Fig. 1*). Complete line-shape analysis of the variable-temperature ^{13}C-NMR spectra (*Fig. 6,a*) was achieved with the following exchange matrix elements: $(a,a) = (d,d) = -k_1/2$; $(b,b) = -k_1$; $(a,b) = (b,a) = (b,d) = (d,b) = k_1/2$; $(c,c) = -k_2$; $(d,d) = -k_2/2$; $(c,d) = k_2$; $(d,c) = k_2/2$; $(g,g) = -k_3/2$; $(e,e) = -k_3$; $(g,e) = k_3/2$; $(e,g) = k_3$ where k_1, k_2, and k_3 are the rate constants of the merry-go-round and the two rotations at one metal centre, respectively. *Eyring* regression of $\ln(k_i/T)$ *vs.* $1/T$ gave the following free enthalpies of activation at 298 K: $\Delta G_1^{\ddagger} = 42.6 \pm 0.4$, $\Delta G_2^{\ddagger} = 47.0 \pm 0.4$, and $\Delta G_3^{\ddagger} = 58.0 \pm 0.8$ kJ mol^{-1}.

Cluster **2** was prepared by a similar procedure as for **3** [2]. Its ^1H-NMR spectrum in solution (see *Exper. Part*) indicates the presence of a major isomer (93%) having probably the same conformation of the coordinated bidentate ligand as that found in the solid, and of a minor isomer with the inverted arrangement of the H–C–Me group. The following results concern only the major isomer.

The limiting ^{13}C-NMR spectrum of a sample of **2** enriched in ^{13}CO (*ca.* 30%) consists of 7 resonances at 223.5(*a*), 203.8(*b*), 179.5(*f*), 171.3(*d*), 163.8(*c*), 162.2(*e*), and 156.7(*g*) ppm with relative intensities 1:2:2:1:1:1:2 in order of decreasing δs. The first two resonances appear in the region characteristic of bridging COs, the next two in the region of radial COs, and the last resonance shows a pseudo-*trans* coupling with ^{31}P, indicating C_s symmetry. Therefore, the geometry of the ground state of **2** in solution is the same as of the structure in the solid. As expected, the bite angle of the bidentate ligand

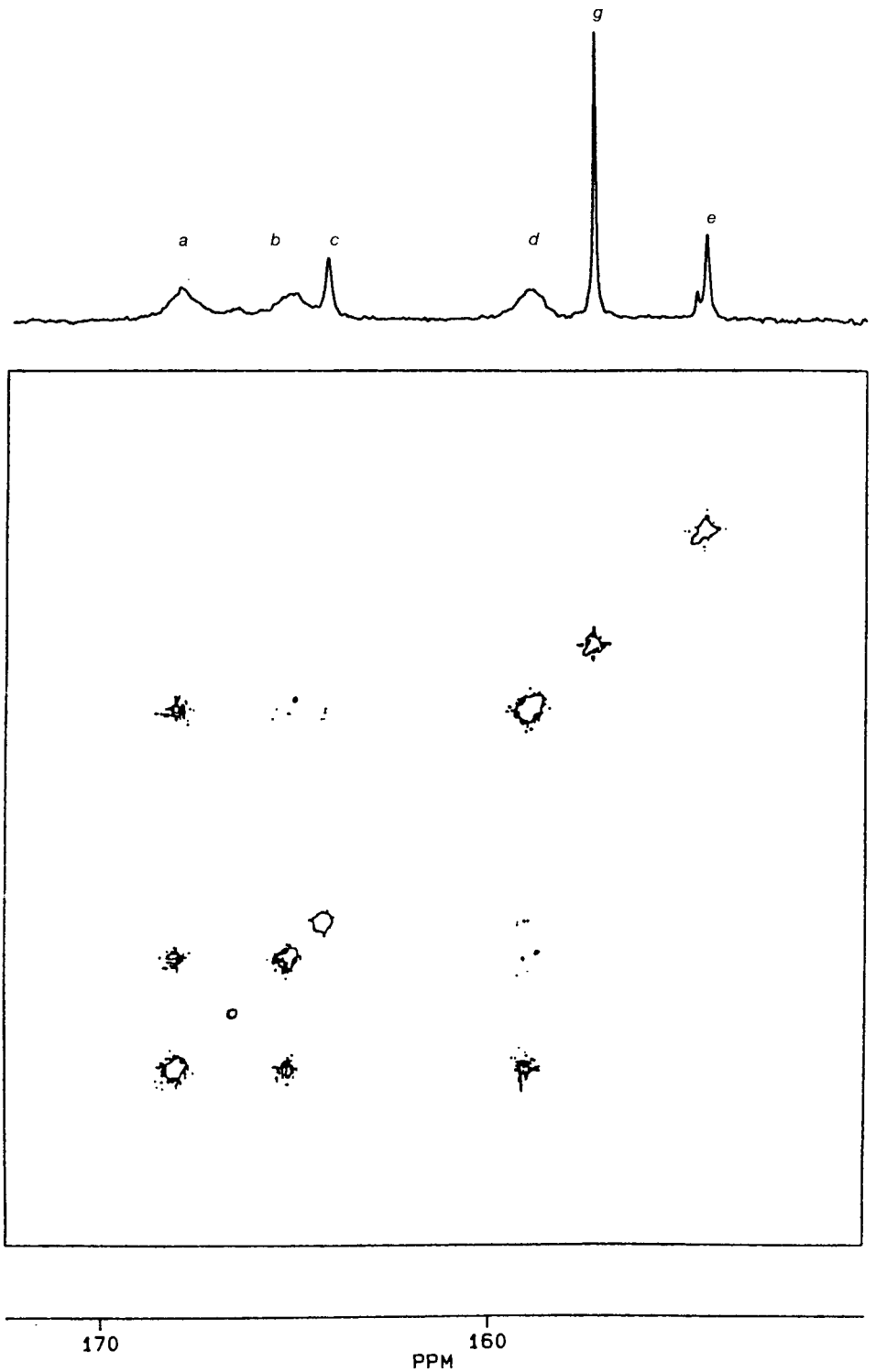

Fig. 5. *2D-EXSY Spectrum of* **1** CD_2Cl_2 *at 215 K* (mixing time 20 ms)

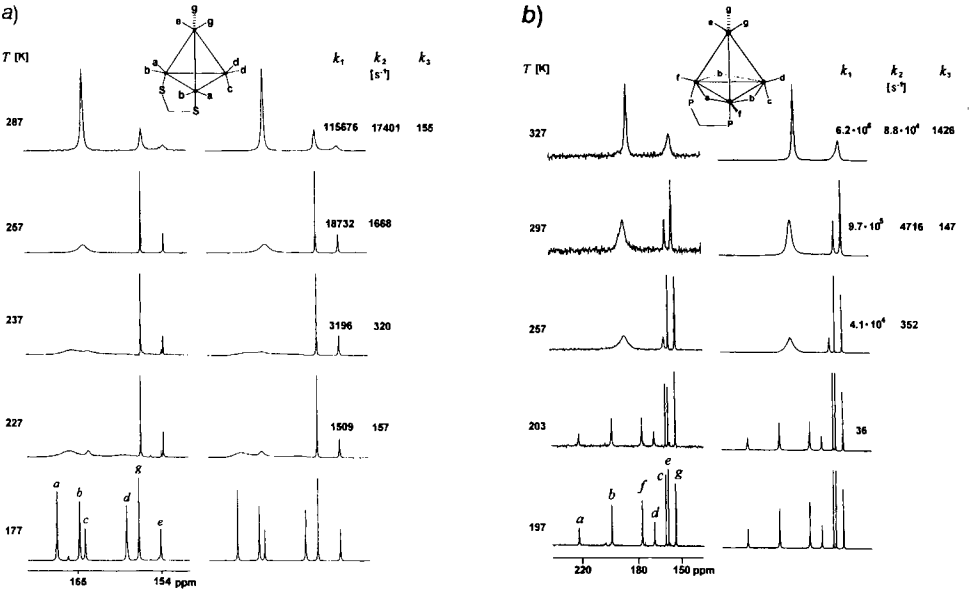

Fig. 6. *Variable-temperature* ^{13}C*-NMR spectra of* a) **1** *in* CD_2Cl_2 *and* b) **2** *in THF*

in **2** is about the same as that in $[Ir_4(CO)_{10}(\mu_2\text{-}Ph_2PCH_2PPh_2)]$[2] ($\Delta\delta(^{31}P) = -30.5$ and -29.5 ppm, resp.), but is quite different from that in **3** (-3.1 ppm [2]).

Upon raising the temperature, the signals at 223.5, 203.8, 179.5, and 171.3 ppm start to broaden and, at 215 K, the 2D-EXSY spectrum of **2** is similar to that reported for **3** [2]. Therefore, the site-exchange process of lowest energy of activation is the merry-go-round involving COs *a*, *b*, *f*, and *d* (rate constant k_1). At *ca.* 247 K, the signal at 163.8 ppm due to the CO *c* starts to broaden (rate constant k_2), and above 287 K, the two site exchange involving COs *g* and *e* becomes apparent. Line-shape analysis of the variable-temperature ^{13}C-NMR spectra of **2** in THF (*Fig. 6, b*), followed by *Eyring* regression of $\ln(k_i/T)$ *vs.* $1/T$ gave the following free enthalpies of activation: $\Delta G_1^{\ddagger} = 38.7 \pm 0.4$, $\Delta G_2^{\ddagger} = 50.4 \pm 0.4$, and $\Delta G_3^{\ddagger} = 60.1 \pm 0.6$ kJ mol^{-1}. The successive fluxional processes taking place in **1** and **2** are clearly the same. Therefore, the respective ground-state geometries merely correspond to relative minima of the same kinetic profile. One may conclude that the unobserved intermediate of the merry-go-round in **2** and **3** has a geometry with all ligands terminal (*Fig. 7*), and suggest that the transition state of the merry-go-round has a semi-bridged geometry, as proposed for $[Ir_4(CO)_9(\mu_3\text{-}1,3,5\text{-}trithiane)]$[4].

The energy barrier of the merry-go-round in **2** and $[Ir_4(CO)_{10}(\mu_2\text{-}Ph_2PCH_2PPh_2)]$ is much lower ($\Delta G_1^{\ddagger} = 38.7$ and 38.0 kJ mol^{-1}, respectively) than in **3** (53.9 kJ mol^{-1} [2]). As discussed in the preceding crystallographic part, the tilt angle of a $Ir_2(\mu\text{-}CO)$ plane with respect to the basal plane, *i.e.*, for the bridging CO *a* (C(12) in *Fig. 2* and *3*) has values of 12 and 3° in **2** and **3**, respectively, while radial COs *f* deviate from that plane by 18 and 27° in **2** and **3**, respectively. In the CO-bridged isomer of $[Ir_4(CO)_9(\mu_3\text{-}1,3,5\text{-}trithiane)]$[4], the tilt angles of the bridging and radial COs have values of 8 and 18°, respectively, while in the unbridged isomer the tilt angles of the corresponding six COs

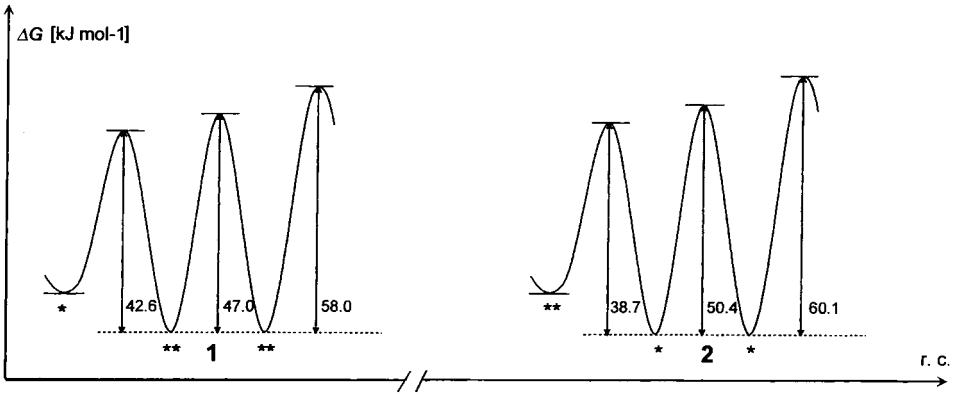

Fig. 7. *Comparative kinetic profiles of the site exchanges in* **1** *and* **2**. * = CO-Bridged isomer; ** = CO-unbridged isomer; r.c. = reaction coordinate.

have a mean value of 13°. It may, therefore, be proposed that on opening bridges in the merry-go-round, the bridged COs move up towards the apical Ir-atom, whereas the radial COs move away from that atom. Assuming also an average tilt angle of 13° for the open forms of **2** and **3**, the sum of the relative vertical displacements of COs *a* and *f* are significantly smaller in **2** (6° than in **3** (24°). In addition to this, the basal CO_2 experience less steric hindrance from the Ph groups in **2** than in **3**. Both factors which originate in the different bites of the bidentate ligands should facilitate the merry-go-round in the former cluster, as observed experimentally.

The same structural factor of the ground state may also explain the lower barrier to rotation of the apical COs in **2** ($\Delta G_3^{\ddagger} = 60.1$ kJ mol^{-1}) relative to **3** (> 80 kJ mmol^{-1}). Upon rotation, the apical COs must pass through an eclipsed position with respect to the three terminal COs of the basal face. As shown by the crystal structures, the latter COs are further away from the apical COs in **2**, thus lowering the rotational barrier in **2** relative to **3**.

We thank the *Swiss National Science Foundation* and *M.U.R.S.T.* (Italy) for financial support.

Experimental Part

1. *General.* See [1], also for 2D-EXSY and variable-temperature ^{13}C-NMR spectra.

2. *Syntheses.* For $NEt_4[Ir_4(CO)_{11}Br]$, see [6]; for tetrahedro-*tri-μ-carbonylheptacarbonyl{μ-{propane-1,3-diyl-bis[diphenylphosphine]-κP: κP′}}tetrairidium* (**3**), see [2]; for enriched derivatives, see [7].

tetrahedro-*Decacarbonyl{μ-[1,1-bis(methylthio-κS)ethane]}tetrairidium* ($[Ir_4(CO)_{10}(\mu_2\text{-}(MeS)_2CHMe)]$; **1**). A soln. of $NEt_4[Ir_4(CO)_{11}Br]$ (450 mg, 0.35 mmol) and 1,1-bis(methylthio)ethane [8] (213 μl, 1.66 mmol) in CH_2Cl_2 (100 ml) was stirred in the presence of $AgBF_4$ (80 mg, 0.41 mmol) for 3 h at 257 K under Ar. The yellow-brown suspension was filtered through a precooled pad of silica gel (2.5 · 20 cm) and eluted with cold CH_2Cl_2. The yellow soln. was stirred for 25 h at 313 K. The solvent was evaporated and the residue dissolved in CH_2Cl_2 (5 ml) and separated by prep. TLC (silica gel, CH_2Cl_2/pentane 1:1) to give two yellow fractions. Recrystallization from CH_2Cl_2/heptane gave **1** (226 mg, 55%) and ($[Ir_4(CO)_{11}((MeS)_2CHMe\text{-}\kappa S)]$ (50 mg, 12%). The latter compound (IR (CH_2Cl_2): 2094*s*, 2056*vs*, 2032*vs*, 2014(sh), 1960*w*, 1845*w*, 1821*w* (CO)) is unstable in soln. at r.t., as it disproportionated into insoluble $[Ir_4(CO)_{12}]$ and **1**. **1**: IR (CH_2Cl_2, 298 K): 2082*s*, 2043*vs*, 2023*vs*, 1986*m*, 1962*m*, 1830*w*, 1788*w* (CO). ^{1}H-NMR (CD_2Cl_2, 270 K): 4.00 (*q*, ^3J(H,H) = 6.35, 1 H); 2.84 (*s*, 6 H); 1.23 (*d*, 3 H). ^{13}C-NMR (CD_2Cl_2, 177 K): 167.7 (1, *a*); 164.9 (2, *b*); 164.1 (1, *c*); 158.8 (2, *d*); 157.2 (2, *g*); 154.3 (1, *e*). Anal. calc. for $C_{14}H_{10}Ir_4O_{10}S_2$ (1171.24): C 14.36, H 0.86; found: C 14.40, H 0.96.

tetrahedro-*Tri-μ-carbonylheptacarbonyl{μ-{ethylidenebis[diphenylphosphine]-κP:κP'}}tetrairidium* ($[Ir_4(CO)_{10}(\mu_2\text{-}(Ph_2P)_2CHMe)]$; **2**). A soln. of $NEt_4[Ir_4(CO)_{11}Br]$ (600 mg, 0.47 mmol) in CH_2Cl_2 (100 ml) was added dropwise to a soln. of ethylidenebis[diphenylphosphine] [9] (400 mg, 1.00 mmol) in CH_2Cl_2 (50 ml) at −20°, and stirred for 1 h at −20° and for 4 h at 0°. The solvent was evaporated and the residue washed with cold heptane (3 × 10 ml) and cold MeOH (10 ml). After addition of CH_2Cl_2 and filtration, the crude product was precipitated with MeOH. Recrystallization from CH_2Cl_2/heptane gave **2**. Yellow microcrystals (515 mg, 76%). IR (CH_2Cl_2, 298 K): 2069*vs*, 2037*s*, 2011*vs*, 1988(sh), 1867*vw*, 1835*m*, 1776*m* (CO). ^{1}H-NMR (CD_2Cl_2, 270 K): major isomer (93%): 2.41 (*tq*, 1 H); 0.46 (*dt*, ^3J(H,H) = 7.2, ^3J(P,H) = 12.3, ^2J(P,H) = 15.1, 3 H); minor isomer (7%): 3.63 (*tq*, 1 H); 0.76 (*dt*, ^3J(H,H) = 7.3, ^3J(P,H) = 11.2, ^2J(P,H) = 16.4, 3 H). ^{31}P{^{1}H}-NMR (CD_2Cl_2, 298 K): −37.5 (*s*, 93%); −35.4 (*s*, 7%). ^{13}C-NMR (CD_2Cl_2, 185 K): major isomer 223.5: (*t*, ^2J(C,P) = 10.4, 1 CO, *a*); 203.8 (*t*, ^2J(C,P) = 10.4, 2 CO, *b*); 179.5 (*s*, 2 CO, *f*); 171.3 (*s*, 1 CO, *d*); 163.8 (*s*, 1 CO, *c*); 162.2 (*s*, 1 CO, *e*); 156.7 (*t*, ^3J(C,P) = 16.8, 2 CO, *g*); minor isomer: 228.1 (^2J(C,P) = 10.2); 206.9 (^2J(C,P) = 10.4); 178.3; 170.7; 161.7; 160.5; 157.4. Anal. calc. for $C_{36}H_{24}Ir_4O_{10}P_2$ (1447.41): C 29.87, H 1.67; found: C 29.50, H 1.81.

The major isomer has most probably an for steric reasons the same conformation of the H–C–Me group as that observed in the solid, with the unique H-atom located under the basal face.

3. *Crystal-Structure Determination.* **1**: Orthorhombic, space group *Pbca*; a = 14.132(3) Å, b = 16.386(3) Å, c = 20.189(4) Å, V = 4675(2) Å^3, Z = 8, μ = 22.923 mm^{-1}, F(000) = 4112. The diffraction intensities were collected at r.t. on a *Stoe IPDS* diffractometer; MoK_α (λ 0.71073 Å), graphite-monochromatized, θ range 2.02–24.02°, index range $-16 \le h \le 16$, $-18 \le k \le 18$, $-22 \le l \le 22$; 28105 reflections collected, 3656 independent reflections (R_{int} 5.55%); refinement method: full-matrix least-squares on F^2; 272 parameters were refined to final indices R 2.17%, R_w 4.78%; goodness of fit 0.393, largest difference peak 0.870 e Å^{-3}; largest difference hole −0.848 e Å^{-3}. The Ir-atoms were localized using direct methods, and the remaining S-, O- and C-atoms were localized on the subsequent *Fourier* difference maps. For the calculations, the SHELXTL 5.05 and XTAL 3.2 program packages were used. Selected bond lengths [Å] and [°]: Ir(1)–Ir(2) 2.6515(6), Ir(1)–Ir(3) 2.7025(7), Ir(1)–Ir(4) 2.6621(6), Ir(2)–Ir(3) 2.7062(6), Ir(2)–Ir(4) 2.6692(7), Ir(3)–Ir(4) 2.6858(7), Ir(1)–S(1) 2.377(2), Ir(2)–S(2) 2.386(3), C(1)–C(2) 1.54(2), Ir–C (mean) 1.899(12), S–C (mean) 1.834(12), CO (mean) 1.133(12); Ir(3)–Ir(1)–S(1) 96.04(6), Ir(2)–Ir(1)–S(1) 93.62(6), Ir(4)–Ir(1)–C(12) 102.6(3), Ir(4)–Ir(1)–C(11) 98.6(3), S(1)–Ir(1)–C(11) 99.2(4), S(1)–Ir(1)–C(12) 97.4(3), Ir(3)–Ir(2)–S(2) 97.03(6), Ir(4)–Ir(2)–C(21) 96.9(3), Ir(4)–Ir(2)–C(22) 103.4(4), S(2)–Ir(2)–C(21) 99.9(3), S(2)–Ir(2)–C(22) 97.8(4), Ir(4)–C(3)–C(31) 99.7(4), Ir(4)–Ir(3)–C(32) 93.4(4), Ir–Ir–Ir (mean) 60.0(5), S(1)–C(1)–S(2) 105.1(6).

2; Triclinic, space group *P*-1; a = 10.898(3) Å, b = 12.712(4) Å, c = 14.998(6) Å, α = 80.11(2)°, β = 86.12(2)°, γ = 65.46(2)°, V = 1861.9(10) Å^3, Z = 2, μ = 14.39 mm^{-1}. The diffraction intensities were collected at r.t. on a *Siemens-P4* diffractometer as for **3**; MoK_α (λ 0.71073 Å), graphite-monochromatized, 2θ range 2.0–50.0°, scan type ω, index range $-14 \le h \le 14$, $-16 \le k \le 16$, $0 \le l \le 19$; 8971 reflections collected, 8465 independent reflections (R_{int} 2.9%), absorption correction applied according to [10]. The Ir- and P-atoms were localized using direct methods, and the remaining atoms were localized on the subsequent *Fourier* difference maps. The quantity minimized was $\sum w(F_o - F_c)^2$ with $w^{-1} = \sigma^2(F) + 0.01\ F^2$. For the H-atoms (calculated), the riding model with fixed isotropic U was used; 350 parameters were refined to final indices R 6.7%, R_w 8.3%; goodness of fit 0.77, largest difference peak 3.0 e Å^{-3}; largest difference hole −1.6 e Å^{-3}. For the calculations, the SHELXTL IRIS [11] program package was used. Selected bond lengths [Å] and angles [°]: Ir(1)–Ir(2) 2.701(1), Ir(1)–Ir(3) 2.725(1), Ir(1)–Ir(4) 2.746(1), Ir(2)–Ir(3) 2.751(1), Ir(2)–Ir(4) 2.726(2), Ir(3)–Ir(4) 2.725(2), Ir(1)–P(1) 2.315(5), Ir(2)–P(2) 2.312(5), P–C(1) (mean) 1.87(1), C(1)–C(2) 1.52(3), Ir–C(bridged) (mean) 2.10(1), Ir–C(terminal) (mean) 1.91(1); P(1)–Ir(1)–C(11) 96.7(6), P(1)–Ir(1)–C(12) 94.6(5), P(1)–Ir(1)–C(31) 101.7(6), P(1)–Ir(1)–Ir(2) 95.3(1), P(1)–Ir(1)–Ir(3) 100.9(1), Ir–Ir–C(bridged) (mean) 49.6(5), Ir(4)–Ir(1)–C(11) 109.4(5), Ir(4)–Ir(1)–C(12) 77.6(5), Ir(4)–Ir(1)–C(31) 80.3(5), P(2)–Ir(2)–Ir(1) 96.9(1), P(2)–Ir(2)–Ir(3) 104.0(1), Ir(4)–Ir(2)–C(12) 77.1(5), Ir(4)–Ir(2)–C(21) 104.6(6), Ir(4)–Ir(2)–C(32) 86.0(6), Ir(4)–Ir(3)–C(31) 80.2(6), Ir(4)–Ir(3)–C(32) 82.7(6), Ir(4)–Ir(3)–C(33) 89.5(7), Ir–C(bridged)–Ir (mean) 80.8(6), Ir–Ir–Ir (mean) 60.0(1), Ir(1)–P(1)–C(1) 113.5(5), Ir(2)–P(2)–C(1) 111.9(6), P(1)–C(1)–P(2) 117.4(10), P–C(1)–C(2) (mean) 115.0(7).

3: Monoclinic, space group $P2_1/n$; a = 13.015(6) Å, b = 22.61(2 Å, c = 14.980(8) Å, β = 90.99(2)°, V = 4408(4) Å^3, Z = 4, μ = 12.2 mm^{-1}; 2θ range 2.0–50.0°, scan type ω, index range $-15 \le h \le 15$, $0 \le k \le 26$, $0 \le l \le 17$; 7989 reflections collected, with 7683 independent reflections (R_{int} 7.9%); absorption correction applied according to [10]. The Ir- and P-atoms were localized using direct methods, and the remaining atoms were localized on the subsequent *Fourier* difference maps. On the maps, a molecule of solvent C_6H_6 appeared, and it was refined with occupancy factor 0.5. The quantity minimized was $\sum w(F_o - F_c)^2$ with $w^{-1} = \sigma^2(F) + 0.02\ F^2$. For the H-atoms (calculated), the riding model with fixed isotropic U was used; 382 parameters were refined to

final-R 7.5%, R_w 9.7%; goodness of fit 0.66, largest difference peak 3.5 e Å^{-3}; largest difference hole −1.7 e Å^{-3}. Selected bond lengths [Å] and angles [°]: Ir(1)–Ir(2) 2.775(2), Ir(1)–Ir(3) 2.743(2), Ir(1)–Ir(4) 2.726(2), Ir(2)–Ir(3) 2.740(2), Ir(2)–Ir(4) 2.722(2), Ir(3)–Ir(4) 2.722(2), Ir(1)–P(1) 2.311(6), Ir(2)–P(2) 2.326(6), P–C(chain) (mean) 1.86(1), Ir–C(bridged) (mean) 2.08(6), Ir–C(terminal) (mean) 1.90(1); P(1)–Ir(1)–C(11) 92.4(9), P(1)–Ir(1)–C(12) 101.2(7), P(1)–Ir(1)–C(31) 93.6(7), P(1)–Ir(1)–Ir(2) 114.2(2), P(1)–Ir(1)–Ir(3) 109.3(2), P(1)–Ir(1)–Ir(4) 68.8(2), Ir–Ir–C (bridged) (mean) 48.5(6), Ir(4)–Ir(1)–C(11) 97.9(9), Ir(4)–Ir(1)–C(12) 81.1(7), Ir(4)–Ir(1)–C(31 81.1(7), P(2)–Ir(2)–Ir(1) 113.7(2), P(2)–Ir(2)–Ir(3) 109.4(2), Ir(4)–Ir(2)–C(12) 81.4(6), Ir(4)–Ir(2)–C(21) 100.1(8), Ir(4)–Ir(2)–C(32) 80.0(7), Ir(4)–Ir(3)–C(31) 79.5(7), Ir(4)–Ir(3)–C(32) 78.1(6), Ir(4)–Ir(3)–C(33) 99.0(10), Ir–C(bridged)–Ir (mean) 82.9(9), Ir–Ir–Ir (mean) 60.0(5), Ir(1)–P(1)–C(1) 116.1(8), Ir(2)–P(2)–C(3) 116.5(9), P(1)–C(1)–C(2) 114.4(19), C(1)–C(2))–C(3) 116.3(26), P(2)–C(3)–C(2) 109.3(19).

Crystallographic data (excluding structure factors) for the structures **1**–**3** are available from *R.R.* and will be deposited with the *Cambridge Crystallographic Data Center*. Copies of the data can be obtained, free of charge, on application of the *CCDC*, 12 Union Road, Cambridge CB2 1EZ, UK (fax: + 44 (1223) 336 033; e-mail: deposit(*a* ccdc.cam.ac.uk).

REFERENCES

[1] A. Strawczynski, C. Hall, G. Bondietti, R. Ros, R. Roulet, *Helv. Chim. Acta* **1994**, *77*, 754.
[2] A. Strawczynski, G. Suardi, R. Ros, R. Roulet, F. Grepioni, D. Braga, *Helv. Chim. Acta* **1993**, *76*, 2210; R. Ros, A. Scrivanti, V. G. Albano, D. Braga, L. Garlaschelli, *J. Chem. Soc., Dalton Trans.* **1986**, 2411.
[3] K. Besançon, G. Laurenczy, T. Lumini, R. Roulet, G. Gervasio, *Helv. Chim. Acta* **1993**, *76*, 2926 and ref. cit. therein.
[4] G. Suardi, A. Strawczynski, R. Ros, R. Roulet, F. Grepioni, D. Braga, *Helv. Chim. Acta* **1990**, *73*, 154; A. Orlandi, U. Frey, G. Suardi, A. E. Merbach, R. Roulet, *Inorg. Chem.* **1992**, *31*, 1304.
[5] P. Ugliengo, D. Viterbo and G. Chiari, *Z. Kristallogr.* **1993**, *207*, 9.
[6] P. Chini, G. Ciani, L. Garlaschelli, M. Manassero, S. Martinengo, A. Sironi, F. Canziani, *J. Organomet. Chem.* **1978**, *152*, C35.
[7] R. Ros, A. Tassan, *Inorg. Chim. Acta* **1997**, *260*, 89.
[8] M. L. Wolfrom, J. V. Karabinos, *J. Am. Chem. Soc.* **1944**, *66*, 909; G. R. Pettit, I. B. Douglass, R. A. Hill, *Can. J. Chem.* **1964**, *42*, 2357.
[9] C. S. Kraihanzel, P. K. Maples, *J. Organomet. Chem.* **1976**, *117*, 159.
[10] A. C. T. North, D. C. Phillips and F. S. Mathews, *Acta Crystallogr., Sect. A* **1968**, *24*, 351.
[11] G. M. Sheldrick, 'SHELXTL IRIS', Siemens Analytical X-ray Instruments Inc., Madison, WI, 1990.

Received January 9, 1998